Surface & Coatings Technology 369 (2019) 31–43

Contents lists available at ScienceDirect

Surface & Coatings Technology

journal homepage: www.elsevier.com/locate/surfcoat

Automatic remelting and enhanced mechanical performance of a plasma sprayed NiCrBSi coating

Liang-Yu Chen[a,b], Haiyang Wang[a], Cuihua Zhao[c], Sheng Lu[a,*], Ze-Xin Wang[a], Jin Sha[a], Shujin Chen[a], Lai-Chang Zhang[b,*]

[a] School of Materials Science and Engineering, Jiangsu University of Science and Technology, Zhenjiang, Jiangsu 212003, China
[b] School of Engineering, Edith Cowan University, 270 Joondalup Drive, Joondalup, Perth, WA 6027, Australia
[c] Guangxi Key Laboratory of Processing for Non-ferrous Metals and Featured Materials, Nanning 530004, Guangxi, PR China

ARTICLE INFO

Keywords:
NiCrBSi
Plasma spraying
Remelting
Hardness
Coating adhesion
Wear

ABSTRACT

Thermal sprayed NiCrBSi coatings often have some shortcomings such as poor cohesion and adhesion, which degrade their properties and are expected to be eliminated by the remelting process. However, there is still a lack of remelting methods combining the advantages of reliability, reproducibility and low-cost. This work developed a remelting method to remelt the as-sprayed NiCrBSi by plasma gun in an automatic mode using optimized parameters. The remelting process reduces the porosity, eliminates the lamellar boundaries and promotes the formation of metallurgical bonding at the coating/substrate interface. Therefore, the hardness (803 $HV_{0.5}$) and bonding strength (165 MPa) of the remelted NiCrBSi coating are about 22% and 516% higher than the corresponding ones of the as-sprayed NiCrBSi counterpart (hardness: 657 $HV_{0.5}$; bonding strength: 32 MPa). The remelted NiCrBSi coating also exhibit significantly enhanced wear resistance compared with the substrate and as-sprayed one. Comparison between the remelted NiCrBSi coatings prepared by various remelting methods indicates that the remelting process used in this work is prominently useful for wider industrial applications since it is reliable, reproducible and convenient.

1. Introduction

Ni-based alloys are well known because of their good resistance to wear, corrosion and high-temperature oxidation; hence Ni-based alloys are commonly used as coating materials for industrial applications [1–4]. Among the Ni-based alloy coatings, NiCrBSi alloy is widely used in engines, piston rods, and boilers because of its high wear and corrosion resistance [5,6]. Generally, NiCrBSi coating can be rapidly synthesized by thermal spraying technologies, including atmospheric plasma spraying (APS) [7–9], flame spraying (FS) [10,11] or high velocity oxygen fuel spraying (HVOFS) [12,13]. These technologies synthesize the NiCrBSi coatings by melting the feedstock particles into droplets and impinging the droplets on a substrate in a layer-wise method [14]. Therefore, the prepared NiCrBSi coatings always display a typical lamellar microstructure. Unfortunately, thermal spraying deposited NiCrBSi coatings still have a considerable number of drawbacks. For example, there are still many particles in an unmelted or semi-melted state; therefore the pores and lamellar boundaries are inevitably produced during the deposition of these unmelted or semi-melted particles, which degrades the wear and corrosion resistance of NiCrBSi coatings [15,16]. Meanwhile, due to the mechanical interlocking at the coating/substrate interface, the NiCrBSi coatings usually have poor adhesion to the substrate [10].

As such, several remelting methods are developed for eliminating these drawbacks, such as flame remelting (FR) [10,11,17], laser remelting (LR) [10,18–20], furnace remelting (FUR) [16,21], electric resistance remelting (ERR) [10], and tungsten inert gas remelting (TIG) [22–25]. The remelting process employs a heat source to heat the as-sprayed NiCrBSi coating until the temperature exceeds the remelting point of NiCrBSi alloy. During the remelting process, the flaws (such as pores and lamellar boundaries) are significantly reduced due to the good fluidity of the NiCrBSi alloy [26]. Meanwhile, the interdiffusion between the coating and the substrate is enhanced at high temperature, thereby forming a metallurgical bonding at the coating/substrate interface [27]. Previous work in the literature indicates that the performance of the as-sprayed NiCrBSi coatings has been substantially improved by the remelting methods mentioned above [10,16,18,24,28]. Serres et al. [18] investigated the plasma sprayed NiCrBSi coating remelted by laser and found that the wear rate of the laser remelted NiCrBSi coating decreases by about 50% than that of the as-sprayed

* Corresponding authors.
E-mail addresses: lusheng_ktz@just.edu.cn (S. Lu), l.zhang@ecu.edu.au, lczhangimr@gmail.com (L.-C. Zhang).

https://doi.org/10.1016/j.surfcoat.2019.04.052
Received 7 February 2019; Received in revised form 3 April 2019; Accepted 15 April 2019
Available online 16 April 2019
0257-8972/

one. Li et al. [24] also found that the TIG remelted NiCrBSi coating has a higher hardness and lower friction coefficient than the as-sprayed counterpart. Bergant et al. [16] pointed out that the furnace remelting process significantly reduces the pores and lamellar boundaries of the as-sprayed NiCrBSi coating, thereby decreasing the permeation paths for the electrolyte and increasing the corrosion resistance. Houdková et al. [10] prepared flame sprayed and high velocity oxygen fuel sprayed NiCrBSi coatings and remelted them by flame, electric resistance, and laser. The results showed that all the remelted coatings exhibit improved wear resistance and hardness irrespective of the remelting methods. Therefore, one can conclude that the remelting process is a useful way to enhance the properties of the as-sprayed NiCrBSi coatings.

Although the remelting process has many advantages for the NiCrBSi coatings, there exist apparent limitations of the remelting methods used for industrial applications. For example, manually remelting NiCrBSi coatings on large workpieces by the flame gun is an extremely heavy workload for the operators. It also should be pointed out that the quality of the manually remelted NiCrBSi coatings mainly depends on the experience of the operators, hence the reliability of the manually remelted NiCrBSi coatings may not be guaranteed [28]. Furnace remelting method strictly restricts the size of the remelting workpiece due to the limited size of the furnace chamber [16]. Although laser remelting is a fast and reliable method to remelt the as-sprayed NiCrBSi coatings [20], the laser equipment is much expensive for both purchase and maintenance [29,30]. Hence, it can arise vast additional expenses for laboratory or factory. Tungsten inert gas remelting and electric resistance remelting also have the same limitations on the workpiece size, additional equipment or operators [10,22]. Therefore, an open question arises: is there a common and simply method used for the remelting process as well as the quality of the remelted NiCrBSi coatings? Unfortunately, there is still a lack of existing literature to answer such a question. Therefore, a remelting method has been developed to remelt the plasma-sprayed coating using plasma gun in an automatic mode. This method has some advantages: (i) no size limitation (the same working range for both spraying and remelting); (ii) high reliability of the quality of the remelted coatings (fixed remelting processing parameters); (iii) no extra equipment needed (using the plasma gun); and (iv) wider applications (various processing parameters for workpieces with different size). After optimizing the processing parameters, a plasma sprayed-remelted NiCrBSi coating is successfully prepared and resultant coating possesses enhanced mechanical properties compared to the as-sprayed counterpart.

In this work, the preparation of the plasma sprayed-remelted NiCrBSi coating was reported in detail. Phase constituents, microstructures and mechanical properties (including hardness, coating adhesion and wear performance) of the NiCrBSi coatings before and after remelting were systematically characterized. Since there is no universal method to test the coating adhesion over 70 MPa [31], a dual tool was designed to test the bonding strength of the remelted samples. Furthermore, a comparison among the different remelting methods was conducted.

2. Experimental

2.1. Sample preparation

Since plasma spraying technology is widely used to synthesize protective coatings on workpieces (such as turbine blade and pistons), which are always made of stainless steels, an annealed 2Cr13 stainless steel with the dimension of 40 × 40 × 5 mm was used as substrate in this work. The polished substrate surface was cleaned by acetone to eliminate oil contamination and then treated by grit blasting before spraying. NiCrBSi alloy powder obtained from the BGRIMM Advanced Materials Science and Technology Co., Ltd. was selected as the feedstock material. The raw powder was manufactured by atomization. The particle size of the feedstock ranged from 45 to 109 μm. Before spraying, the powder was dried at 200 °C in a furnace for 2 h. The chemical compositions of the NiCrBSi powder and the 2Cr13 substrate are listed in Table 1.

Table 1
The chemical compositions (in wt%) of NiCrBSi powder and 2Cr13 steel substrate.

Elements	C	Si	B	Cr	Mn	Ti	Fe	Ni
NiCrBSi powder	0.6	4.5	3.0	16.2	–	–	5.3	Bal.
2Cr13 steel substrate	0.2	0.8	–	13.0	0.8	0.2	Bal.	0.6

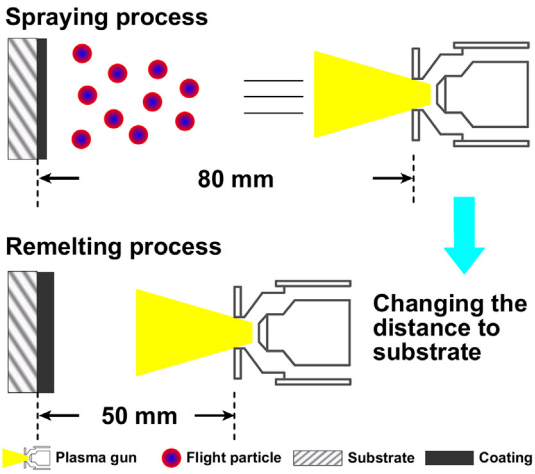

Fig. 1. Schematic illustration of the spraying and remelting process.

The spraying and remelting process were conducted using an SG-100 plasma-spraying torch (Praxair, USA). During spraying, argon was used as the main gas to reduce particle oxidation. As shown in Fig. 1, the remelting process was immediately conducted by the plasma gun in an automatic mode after spraying by changing the gun traverse rate and the distance to substrate. The remelting process was repeated by 3 times. Since NiCrBSi alloy is a self-fluxing alloy, the containing B and Si have the functions of self-deoxygenation and slag formation. These functions can protect the NiCrBSi alloy from oxidation. Therefore, slight oxidation on the surface of the remelted NiCrBSi coatings can be ignored. During the remelting process, the temperature of the coating was recorded by an infrared thermometer and temperature was found to exceed 1500 °C. After remelting, the remelted samples were cooled in air. The as-sprayed and remelted NiCrBSi coatings prepared on the cuboid substrates were used to conduct the microstructural characterization, hardness tests, and wear tests. The detailed spraying and remelting parameters are shown in Table 2.

Table 2
Plasma spraying and remelting parameters selected for depositing NiCrBSi coating.

Parameters	Spraying	Remelting
Voltage (V)	60	60
Current (A)	500	500
Powder feed rate (g/s)	0.3	–
Spray step (mm)	3	3
Gun traverse rate (mm/s)	100	10
Main gas Ar (dm^3/s)	4.1	4.1
Secondary gas N_2 (dm^3/s)	1	1
Feed gas Ar (dm^3/s)	2.1	2.1
Distance to the substrate (mm)	80	50
Number of spray or remelting passes	6	3

2.2. Microstructural characterization

An optical microscope (OM, Zeiss Axioskop2-MAT, Germany), a laser scanning confocal stereomicroscope (OLS4000, Olympus, Japan), a Merlin Compact field emission scanning electron microscope (SEM, Zeiss, Germany), and a JEM-2100F transmission electron microscope (TEM, JEOL Ltd., Japan) equipped with an energy dispersive X-ray spectroscopy (EDS) detector operated at 200 kV were used for microstructural characterizations. The coating samples for OM and SEM observations were mechanically ground with SiC papers up to 2000 grits and then polished to a mirror surface. For TEM characterizations, the coatings were carefully removed from the substrates and ground to about 100 μm thick, then cut into a 3 mm diameter fold and thinned using a twin-jet polishing machine with a mixed solution composed of $HClO_4$: C_4H_9OH: CH_3OH = 6: 39: 55 (in vol%) at a temperature of −30 °C. The crystallographic characteristics of grains were determined by high resolution TEM (HRTEM) and analyzed using the software Digital Micrograph. The phase constituents of the feedstock, the as-sprayed, and the remelted coatings were characterized by X-ray diffraction (XRD, Bruker, D8 Advance A25X diffractometer, Germany) with a scanning range (2θ) of 30–80°, scanning speed of 2°/min and scanning step of 0.02°. The Jade 6.5 software was used to analyze the XRD patterns.

2.3. Mechanical tests

The Vickers hardness was conducted on the cross-section of the as-sprayed and remelted NiCrBSi coatings using a hardness machine (KB30S, Germany). Before the hardness test, the cross-section of the samples was ground and polished. The indentation load was 5 N with the dwell time of 15 s. Each reported hardness value was averaged from at least ten tested points.

The reciprocating ball-on-flat tribological test was conducted at room temperature on the polished surface of the NiCrBSi coating using friction and wear testing machine (Bruker, UMT-2, Germany) without lubrication in air according to ASTM G133-05. The testing parameters were: reciprocating wear track of 3 mm; 20 N load; ZrO_2 ball in 9.5 mm diameter; sliding speed of 5 mm/s or 10 mm/s; and testing time of 1200 s. Three different measurements were carried out to each sample at room temperature. The average wear volumes were measured by a 3D confocal laser microscope (Olympus OLS4000, Japan) at 5 different places on the wear tracks. SEM observations were conducted to observe the morphologies of the wear tracks.

Traditional bonding strength test for examining the coating adhesion was performed in accordance with the commonly used ASTM C633-79 [31]. However, the maximum tested strength was limited by the glue used (less than 70 MPa) [31]. According to previous work [31], the bonding strength would exceed the test limit if the metallurgical bonding was presented at the coating/substrate interface. As such, coating adhesion was tested using a self-designed dual tool as shown in Fig. 2. This tool consisted of three components A, B and C (Fig. 2a). Components A and B could combine together to form a piston structure. The combined components A and B can be placed in the hollow of component C to form a mechanical interlocking. Fig. 2b shows the separated components A and B. Component A was a round cap and component B was a cylinder. The one at end of component B was plugged into a taper shape in order to reduce the friction between components A and B during the bonding strength test. The schematic diagram of the combined components A and B associated with the coating is presented in Fig. 2c. The top of the taper on component B had a diameter of 4 mm. The cylinder part of component B was 7.5 mm in radius. During the bonding strength test, components B and C were fixed in a universal testing machine (CMT5205, America). A loading rate of 165 N/s was employed for the bonding strength test until the coating failed. The ratio of maximum loading and area of taper top was considered as the coating adhesion in this work. The preparation of the bonding strength test samples used the same procedure as the cuboid samples. The fracture morphologies of bonding strength test samples were observed by both stereomicroscopy and SEM.

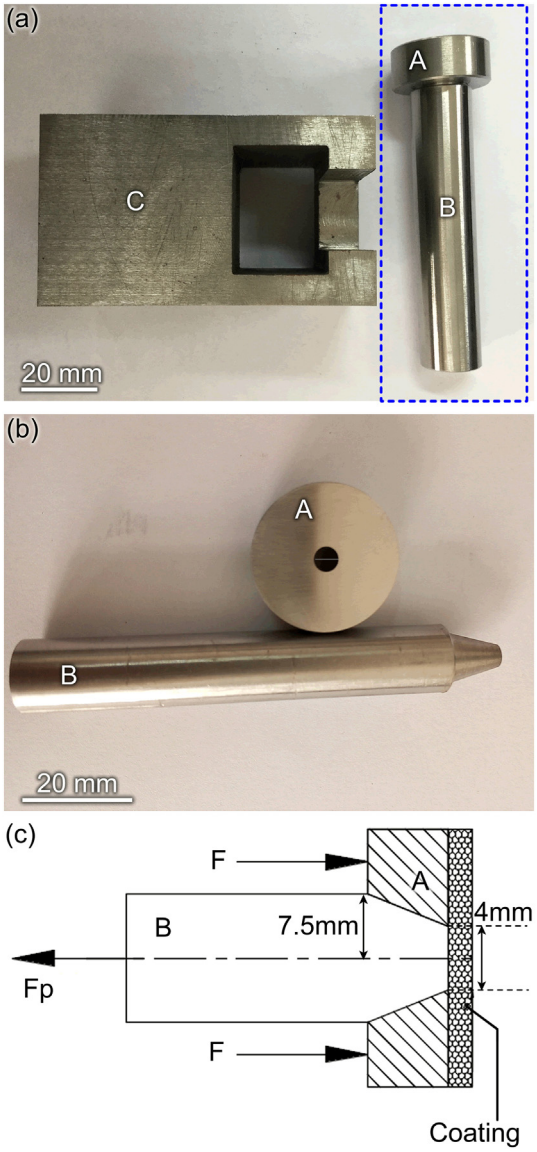

Fig. 2. Images of the dual tool for bonding strength test: (a) three components of the tool consisted of A, B, and C; (b) component A is a round cap and component B is a cylinder with a taper shape end; and (c) schematic diagram of the combined components A and B associated with coating.

3. Results and discussion

3.1. Phase constituents

Fig. 3 shows the XRD patterns of the as-sprayed and remelted NiCrBSi coatings. It is observed that six phases, i.e. γ-Ni, Cr_7C_3, Cr_3C_2, Ni_3B, CrB, and Cr_3B_4, are detected in the as-sprayed coating. Besides the Cr_3B_4, the other five phases can be found in the starting material used [8]. According to the Cr-B phase diagram [32], Cr_3B_4 is a meta-stable phase, which forms due to the fast cooling rate during the deposition [7]. A broaden diffuse diffraction is observed from 40° to 50° in the XRD pattern of the as-sprayed coating, attributing to the amorphous phase and nanocrystalline [33–37]. As many amorphous alloys, the amorphous phase in the as-sprayed NiCrBSi coating also results from the fast cooling rate and exists in a meta-stable state [7,38–41]. The previous

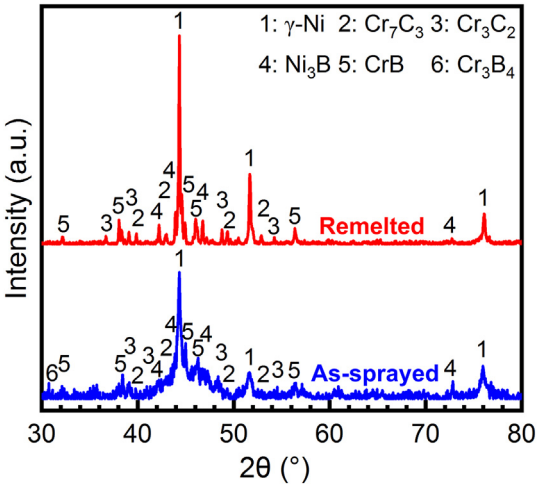

Fig. 3. XRD patterns of the as-sprayed and remelted NiCrBSi coatings.

study demonstrates that the volume fraction of the amorphous phase is about 9.6% in the as-spayed NiCrBSi coating [7]. After remelting, all peaks in the XRD pattern of the remelted coating becomes sharp and the peak of Cr_3B_4 disappears. This elucidates that the remelted NiCrBSi coating has a higher degree of crystallinity and greater grain size, which is attributed to the relatively low cooling rate of the remelted NiCrBSi coating.

3.2. Microstructure features

Fig. 4 reveals the optical images of the as-sprayed and remelted NiCrBSi coatings. The as-sprayed NiCrBSi coating is about 400 μm thick and has a rough surface. Some unmelted particles are found in the as-sprayed NiCrBSi coating associated with large pores. This phenomenon

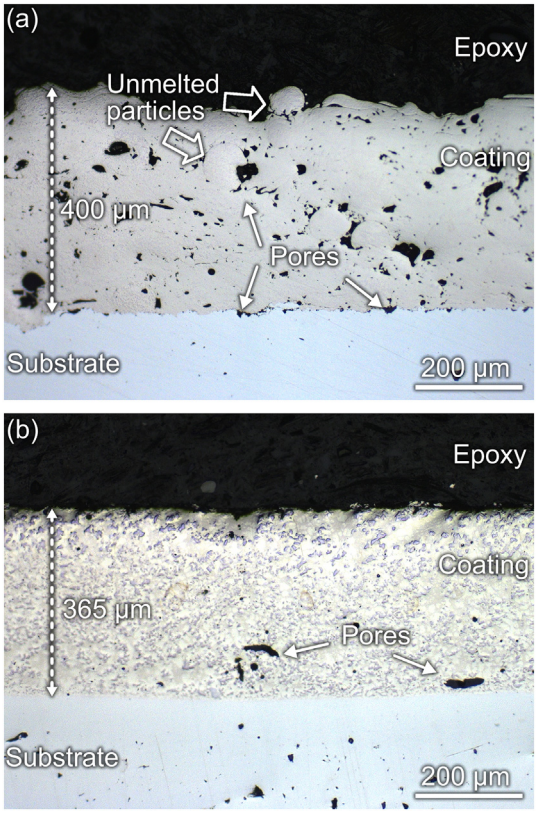

Fig. 4. Optical images of the as-sprayed and remelted NiCrBSi coatings.

results from the loose stacking between unmelted particles [42]. Meanwhile, a lot of relatively small pores are found in the as-sprayed NiCrBSi coating. There are also a considerable number of pores around the coating/substrate interface. Such pores embedded in the coating or around the interface would degrade the cohesion and adhesion of the coating. Hence, a coating with higher porosity often has inferior hardness and corrosion resistance [16,43,44]. In this work, the average porosity of the as-sprayed NiCrBSi coating is about 2.7%. After remelting, the average porosity of the remelted NiCrBSi coating significantly reduces to about 0.8%. Importantly, the pores around the interface of the coating and the substrate are almost absent. The thickness of the remelted NiCrBSi coating also decreases to 365 μm, resulting from the flow of the material and the interdiffusion between the coating and the substrate during the remelting process [16]. Furthermore, the surface of the remelted NiCrBSi coating is much flatter compared with the as-sprayed NiCrBSi counterpart. No unmelted particles are found in the remelted NiCrBSi coating. Therefore, one can conclude that the NiCrBSi coating becomes denser after remelting, which is consistent with the results in literature [10,16].

Detailed SEM microstructures for both the as-sprayed and the remelted NiCrBSi coatings are shown in Fig. 5. Fig. 5a is the surface morphology of the as-sprayed NiCrBSi coating. As seen from the figure, voids and pores are apparent on the surface of the as-sprayed NiCrBSi coating, which can provide diffusion paths for the corrosion species in a corrosive environment [45]. The unmelted and deformed particles on the surface of the as-sprayed NiCrBSi coating increase its roughness. In comparison, the apparent voids and pores disappear after remelting in the remelted NiCrBSi coating and the coating surface becomes relatively flat since the NiCrBSi alloy has good wettability and fluidity [43] (Fig. 5b). Fig. 5c shows a magnified image of the coating/substrate interface of the as-sprayed NiCrBSi coating by SEM in a backscattered electron (BSE) mode. Since BSE imaging generates contrast according to the atomic weight, boride and carbide precipitates can be easily distinguished. Hence, the Cr borides are proved to be dark particles and Cr carbides are considered as light grey particles in literature [21,46]. Overall, the as-sprayed NiCrBSi coating shows a microstructure composed of dark grey polygonal particles (Cr borides), light grey rod-like or irregular precipitates (Cr carbides) and the matrix (Fig. 5c). The Cr borides and Cr carbides are in sub-micron in size. A mechanical interlocking is clearly found on the coating/substrate interface, being accompanied by a large number of caves. Several lamellar boundaries which form by different particles stacking are also observed, indicating a limited interdiffusion among the particles during deposition. Such lamellar boundaries are weak connections between the splats, resulting in a degradation in coating cohesion [47]. By contrast, the caves on the coating/substrate interface of the as-sprayed NiCrBSi coating are substantially eliminated after remelting process (Fig. 5d). The lamellar boundaries in the remelted NiCrBSi coating are also absent. The Cr borides particles have a size range of 1–8 μm and most Cr carbides precipitates are greater than 1 μm in length, which are much larger than those observed in the as-sprayed counterparts, indicating the grain growth during the automatic remelting process. As reported in Ref. [8], a diffusion layer between the coating and the substrate is formed after the automatic remelting process. Therefore, EDS was employed to confirm the element diffusion on the coating/substrate interface. Fig. 5e and f are the EDS results of line scanning for Ni and Fe elements along the yellow arrows marked in Fig. 5c and d. It can be observed in Fig. 5e that there is a sudden drop or increase in the contents of Ni or Fe at the coating/substrate interface, confirming a limited interdiffusion between the coating and the substrate (mechanical interlocking). In general, the NiCrBSi coating having a mechanical interlocking with the substrate possess a limited bonding strength [21,47–50]. Therefore, the remelting process is often employed to obtain a metallurgical bonding at the coating/substrate interface. As seen in Fig. 5f, the contents of Ni and Fe gradually rise or decrease from the coating area to the substrate area, confirming the existence of the diffusion layer (metallurgical

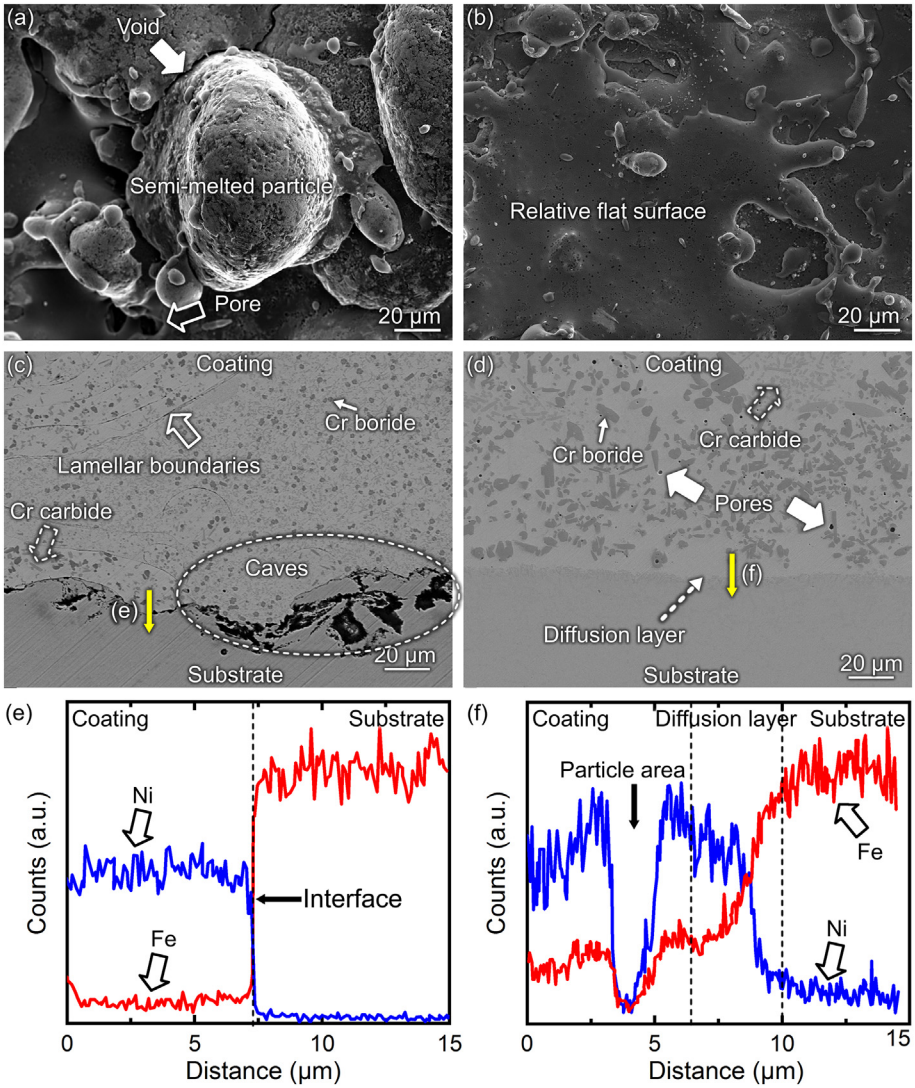

Fig. 5. SEM observations for the surface morphologies of (a) the as-sprayed and (b) remelted NiCrBSi coatings and the interface morphologies of (c) the as-sprayed and (d) remelted NiCrBSi coatings; line scanning profiles of Ti and Fe elements at the interfaces of the (e) as-sprayed and (f) remelted NiCrBSi coatings as marked by yellow arrows in (c) and (d). (For interpretation of the references to color in this figure legend, the reader is referred to the web version of this article.)

bonding) which has a thickness of about 3.5 μm. It was reported that the thickness of the diffusion layer ranges from 5.8 μm to 13.1 μm [8]. Hence, it illustrates that the thickness of the diffusion layer may depend on the surface condition of the substrate. It is speculated that too many caves concentrated on the interface may result in a thin diffusion layer since the caves impede the interdiffusion between the coating and substrate. In the coating area, a common drop is observed in both curves of Fe and Ni, which is considered as the areas of Cr carbides or Cr boride particles. Although the as-sprayed NiCrBSi coating has a considerable number of pores (Fig. 4a), lamellar boundaries and a mechanical interlocking between the coating and the substrate, the automatic remelting process promotes the grain growth and the formation of the metallurgical bonding between the coating and substrate.

In order to further understand the microstructural evolution in a smaller scale, TEM characterization was adopted for both as-sprayed and remelted NiCrBSi coatings. Fig. 6 shows the microstructure features of the as-sprayed NiCrBSi coating. Fig. 6a exhibits a face-centered cubic (FCC) γ-Ni grain in an irregular shape. Some fragmented grains with the chemical compositions (in wt%) of 83.4% Ni, 9.7% Cr, 6.7% Si and 0.2% B are observed as indicated by the dash cycle. It is known that γ-Ni solid solution contains many other alloying elements [10,51]. As seen from the compositions detected (Fig. 6a inset), these grains have much a higher Ni content (83.4 wt%) than the average one in the feedstock (about 70.4 wt%). Hence, these grains could be identified as γ-Ni containing Cr and Si. Fig. 6b reveals an amorphous region embedded with many nanoclusters, which are identified as γ-Ni, Cr_3B_4 and/or Ni_3B by the selected electron diffraction pattern (SAED). The amorphous phase contains 73% Ni, 14% Cr, 2.1% B, 6.6% Si, 3.7% Fe and 0.6% C (all in wt%), similar to the feedstock. Fig. 6c represents the floret-shaped eutectic structure in the as-sprayed coating, which is always found in NiCrBSi coatings [46,52]. The dark grains are identified as Ni_3B and the light grains are γ-Ni. Most grains in the eutectic structure are very fine and the lamellar spacing is below 30 nm. It has been reported that the fine eutectic structure often results from the high heating and cooling rate during solidification of eutectic alloys [53]. Fig. 6d shows a Cr_3B_4 grain of about 623 nm in size observed in the as-sprayed NiCrBSi coating. Meanwhile, lots of stacking faults are presented in the Cr_3B_4 grain. Fig. 6e shows a CrB grain of about 948 nm in size accompanied by multiple twins. Moreover, an amorphous region with lots of precipitates is adjacent to this CrB grain. Compared with nanoclusters in the amorphous region in Fig. 6b, the precipitates in the amorphous region in Fig. 6e are significantly larger in size (up to 100 nm). Precipitation and grain growth can take place at the temperature higher than 440 °C [7]. After deposition, the temperature of

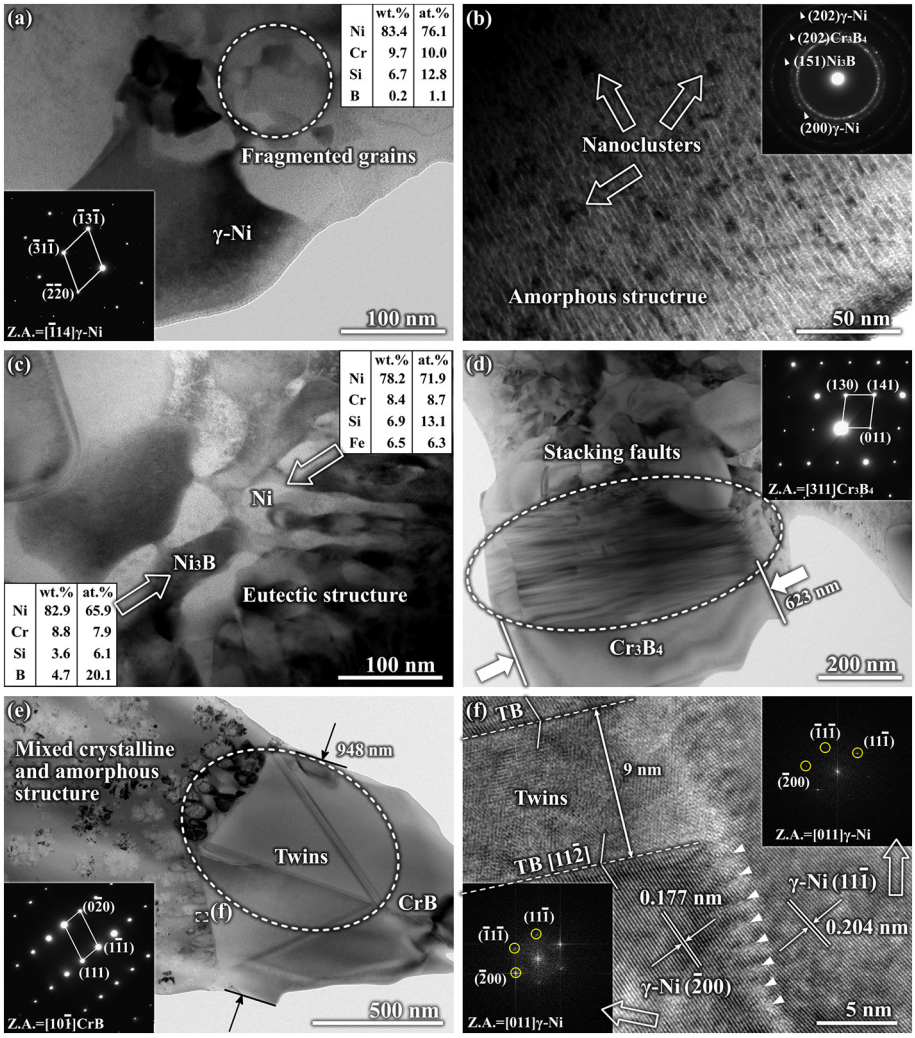

	wt.%	at.%
Ni	83.4	76.1
Cr	9.7	10.0
Si	6.7	12.8
B	0.2	1.1

	wt.%	at.%
Ni	78.2	71.9
Cr	8.4	8.7
Si	6.9	13.1
Fe	6.5	6.3

	wt.%	at.%
Ni	82.9	65.9
Cr	8.8	7.9
Si	3.6	6.1
B	4.7	20.1

Fig. 6. TEM microstructure of the as-sprayed NiCrBSi alloy coating: (a) an irregular-shape γ-Ni grain surrounded by some fragmented grains, (b) amorphous structure embedded with nanoclusters of γ-Ni, Cr_3B_4 and Ni_3B, (c) fine eutectic structure of γ-Ni and Ni_3B grains, (d) a Cr_3B_4 grain with lots of stacking faults, (e) a CrB grain of 948 nm in size and the adjacent mixed crystalline and amorphous region, and (f) HRTEM image of the rectangular region f marked in (e), showing the interface of two γ-Ni grains near a CrB grain. TB means twin boundary. The corresponding selected area electron diffraction patterns are shown in the insets of specific figures.

the NiCrBSi coating is still higher. Crystallization and precipitation may be triggered in the as-sprayed NiCrBSi coatings. Therefore, it is reasonable to observe relatively large precipitates in the amorphous region in the as-spayed NiCrBSi coating. High resolution TEM (HRTEM) was adopted to analyze the rectangle region (f) marked in Fig. 6e. As shown in Fig. 6f, two γ-Ni grains with the same zone axis of [111] are adjacent to each other. The misorientation between these two Ni grains is measured as 44.0°. Hence, a coincidence site lattice grain boundary is clearly indicated by white triangles. Furthermore, micro-twinnings with the coherent twin boundaries of [11$\bar{2}$] are also observed in Fig. 6f, which is commonly reported in cubic structure metals [54]. Combined with the XRD results, one can conclude that the as-sprayed NiCrBSi coating has a complex microstructure since NiCrBSi alloy is a multicomponent alloy.

Fig. 7 reveals the TEM observations for the remelted NiCrBSi coating. Fig. 7a shows two adjacent γ-Ni grains in an elongated shape with curving grain boundaries. The lengths of these γ-Ni grains are greater than 1 μm and their widths are about 200–500 nm. Such γ-Ni grains are much larger than those observed in the as-sprayed NiCrBSi coating. In many locations in the remelted NiCrBSi coating, such morphologies of γ-Ni grains could be found, which is very similar to the reported eutectic structure [46,55,56]. Compared with the Ni grains or eutectic structure in the as-sprayed NiCrBSi coating (Fig. 6a and c), these grains in the remelted NiCrBSi coating are significantly large (Fig. 7a and b). It can readily be understood that the relatively slow cooling rate is maintained a high temperature for the remelted NiCrBSi coating during cooling. Therefore, similar as in other materials [57–61], the grains would grow when they are maintained at a high temperature. Fig. 7b gives the chemical compositions of these two γ-Ni grains and a nearby CrB grain of about 867 nm in size. The γ-Ni grain (indicated by A) is free of Si, whereas the γ-Ni grain (denoted by B) contains about 19.3 at.% Si, much larger than the maximum solution solubility of Si in γ-Ni (10 at.%) [62]. Such a result may stem from an uncompleted Ni-Ni_3Si eutectic reaction. Therefore, it seems that the automatic remelting process with the used parameters could not result in a complete equilibrium microstructure of the remelted NiCrBSi coating in this work, thereby being not favored to the formation of Ni-Ni_3Si eutectic structure. A Cr_3C_2 particle of about 446 nm in size is observed in Fig. 7c. Multiple sets of selected area electron diffraction (SAED) patterns obtained from this particle indicate the existence of stacking faults. Fig. 7d shows a large CrB grain adjacent to a Ni_3B grain. It could be found that plenty of twins are presented in the CrB grain. Fig. 7e and f are the HRTEM images of the rectangular regions (e) and (f) in Fig. 7d. As seen in Fig. 7e, it is found that the angle of 41.4° between two twinned areas consists of (110) and (1$\bar{1}$0) planes. Such {110}⟨1$\bar{1}$0⟩ twins are frequently observed in CrB grains in the remelted

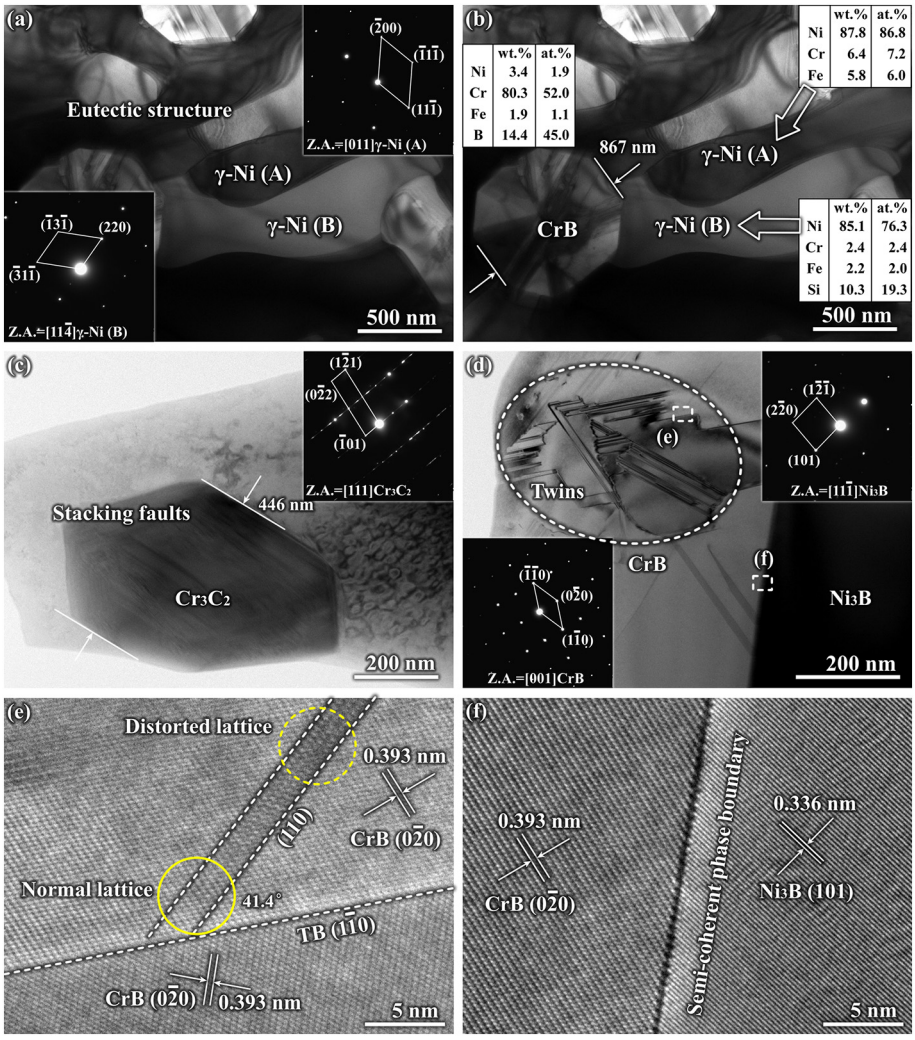

Fig. 7. TEM microstructure of the remelted NiCrBSi alloy coating: (a) floret-shaped eutectic structure of two γ-Ni grains with face-centered cubic structure, (b) chemical compositions of the γ-Ni grains observed in (a) and a nearby CrB particle, where the γ-Ni (A) grain is free of Si and the γ-Ni (B) grain contains about 19.3 at.% Si, (c) a Cr_3C_2 particle with stacking faults embedded in the matrix, (d) a CrB grain with plenty of twins adjacent to a Ni_3B grain, (e) HRTEM image of the rectangular region b in (a), showing that an angle of 41.4° between two twinned areas and (f) a semi-coherent CrB/Ni_3B phase boundary reconciled by interface dislocation with almost no distortion.

NiCrBSi coating [8]. Within the twinned area, both normal lattice and distorted lattice are observed and indicated by the yellow dash cycles, respectively (Fig. 7e). Both normal lattice and distorted lattice are also presented in the twinned area surrounded by {110} planes. Therefore, it could be speculated that the twins in the CrB grain take place via a shuffle-dominated mechanism [63]. The interface of the CrB grain and the Ni_3B is semi-coherent as shown in Fig. 7f. The lattice misfit at the interface is well reconciled by interface dislocations. Hence, no evident distortion is found on both sides of the CrB/Ni_3B interface. Furthermore, no amorphous phase is observed in the remelted NiCrBSi coating. It has been reported that the preparation of the APS-produced coating is attributed to the deposition of the melted or semi-melted particles at a high speed [14]. Therefore, severe plastic deformation takes place between the particles. Combined with the high cooling rate during deposition, the grain growth is also limited in the as-sprayed NiCrBSi coating (Fig. 6b and e). As such, the as-sprayed NiCrBSi coating has a refined microstructure. Conversely, the temperature of the remelted NiCrBSi coating surface was over 1500 °C during remelting. The good wettability and fluidity of NiCrBSi alloy lead to the reduction in porosity, elimination in lamellar boundaries and formation of metallurgical bonding between the coating and the substrate. However, such a high temperature can significantly facilitate the growth of grains in the remelted NiCrBSi coating.

3.3. Hardness

Fig. 8 shows the hardness on the cross-section of the as-sprayed and remelted NiCrBSi coatings. The 2Cr13 stainless steel possesses a lower hardness (about 238 $HV_{0.5}$) than the as-sprayed NiCrBSi coating (633–657 $HV_{0.5}$). Apparently, the hardness of the remelted NiCrBSi coating is 771–825 $HV_{0.5}$, about 22%–26% higher than that of the as-sprayed counterpart. The hardness at the interface of the coating/substrate also increases from 411 $HV_{0.5}$ to 544 $HV_{0.5}$. Combining with the morphologies of the coating/substrate interface for the as-sprayed and

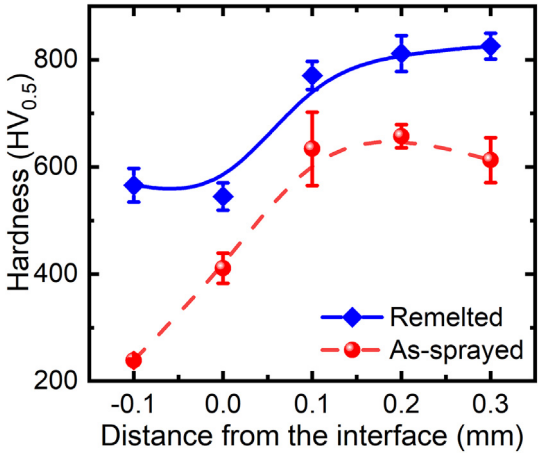

Fig. 8. Hardness on the cross-section of the as-sprayed and remelted NiCrBSi coatings.

remelted NiCrBSi coatings (Figs. 4 and 5), the increase in the hardness of the remelted NiCrBSi coating at the interface is attributed to the elimination of the pores at the of the coating/substrate and the formation of the metallurgical bonding. Similar as in porous metallic materials, the pores play a role in reducing their elasticity modulus and the strength [64–68]. Therefore, the decrease in the porosity enhances the cohesion of the remelted NiCrBSi coating, thereby increasing the hardness. Meanwhile, it is observed that the as-sprayed NiCrBSi contains a certain fraction of the amorphous phase which has been demonstrated to have a lower hardness than the precipitates (e.g. CrB and Ni_3B) in the NiCrBSi coating [7]. Due to the relatively low cooling rate, the amorphous phase is hard to form in the remelted NiCrBSi coating. This deduction has been proved by the XRD results (Fig. 3) and the TEM observation (Fig. 6b). Hence, the decrease in the fraction of the amorphous phase also contributes to enhance hardness. Although the larger grain size (e.g. γ-Ni, boride and carbide grains) (Figs. 5 and 7) in the remelted NiCrBSi coating may have a negative effect on the enhancement of the hardness [7], the combining effect of the elimination of the pores, the reduction of the amorphous phase, and the grain growth leads to 22%–26% increase in the hardness of the remelted NiCrBSi coating (Fig. 8). Furthermore, it is interesting that the hardness at the substrate side increases from 239 $HV_{0.5}$ to 566 $HV_{0.5}$. It is speculated that the elements (such as Ni) in the coating diffuse into the substrate since the concentration of Ni in the substrate in the remelted NiCrBSi coating (Fig. 5f) is greater than that in the as-sprayed counterpart (Fig. 5e), thereby inducing solid solution strengthening. However, the hardness of the substrate would not affect the performance of the coating to some extent.

3.4. Bonding strength

The bonding strength of the as-sprayed and remelted NiCrBSi coatings was measured with the aid of the self-designed dual tool shown in Fig. 2. The bonding strength of the as-sprayed coatings is about 32 MPa (Fig. 9a). It has been reported that the bonding strength of the NiCrBSi coating prepared by various thermal spray technologies ranges from 11 to 66 MPa [21,47–50], depending on the processing parameters and the surface conditions of the substrates used. The value of the bonding strength of the as-sprayed NiCrBSi coating falls in this range, indicating the availability of the method used in this work. Such a low bonding strength may cause the peeling of NiCrBSi coatings during service. After remelting, the bonding strength significantly increases to 165 MPa, which is about 5 times higher than that of the as-sprayed counterpart. Such a high bonding strength can ensure the reliability of the NiCrBSi coating in the service environment. Stereomicroscope was employed to investigate the fracture locations of the bonding strength tested samples, which are shown in Fig. 9b and c. It can be observed that the as-sprayed NiCrBSi coating sample exhibits a relatively flat fracture surface (Fig. 9b). It was reported that a mechanical interlocking is presented at the coating/substrate interface, which has a limited bonding strength [21,47–50]. Therefore, the fracture of the as-sprayed sample is prone to take place at the coating/substrate interface. By contrast, the fracture surface of the remelted NiCrBSi coating sample has a wide range in height difference (Fig. 9c). After remelting, diffusion layer is formed at the coating/substrate interface and the bonding strength increases rapidly. The fractures would take place at the relatively weak connections of the tested sample but not only at the coating/substrate interface. As such, the NiCrBSi coating may be or not be peeled off from the substrate. Hence, if the fracture occurs in the coating, a high terrain would be presented in the stereomicroscopic image. In comparison, if the fracture takes place at the coating/substrate interface, a relatively flat terrain would be exhibited.

In order to investigate the fracture mechanism of the as-sprayed and remelted NiCrBSi coatings, fracture surfaces of the tested samples were examined by SEM associated with EDS. Since there are remnant coating materials in the remelted NiCrBSi coating sample, the SEM examination

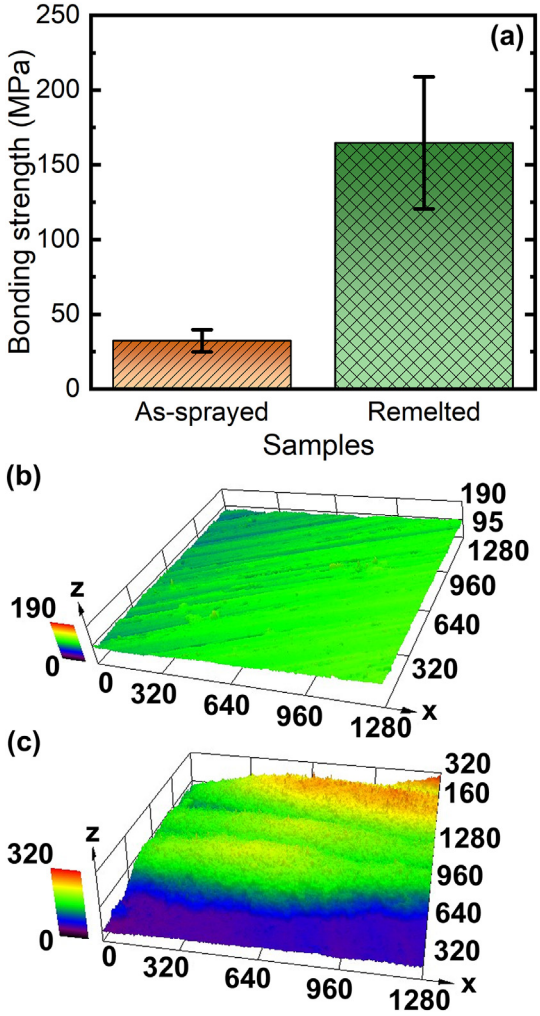

Fig. 9. Bonding strength results and stereomicroscopic fracture morphologies of the as-sprayed and remelted NiCrBSi coatings: (a) bonding strength, (b) stereomicroscopic fracture morphologies of the as-sprayed NiCrBSi coating and (c) stereomicroscopic fracture morphologies of the remelted NiCrBSi coating.

was conducted on its low location in the fracture surface. As seen in Fig. 10a, the as-sprayed NiCrBSi coating, which has a significantly low bonding strength, displays a brittle fracture surface. EDS mappings carried out in the area of yellow dash rectangle show that none Ni is found on the fracture of the as-sprayed NiCrBSi coating. This result indicates that almost no interdiffusion takes place between the coating and the substrate and the as-sprayed NiCrBSi coating is maintained only by mechanical interlocking. Therefore, overall as-sprayed NiCrBSi coating is easily peeled off during the bonding strength test. The fracture of the remelted NiCrBSi coating represents many small dimples, indicating a ductile fracture occurred during the bonding strength test (Fig. 10b). EDS result shows that about 32.6% Ni and 46.5% Fe are presented on the fracture of the remelted NiCrBSi coating. Hence, the fracture takes place in the diffusion layer of the remelted NiCrBSi coating. Such a difference is attributed to the transformation of the mechanical interlocking to the metallurgical bonding at the coating/substrate interface, resulting in a significantly increase in bonding strength. The thickness of the diffusion layer in the remelted NiCrBSi is about 3.5–13.8 μm. It is speculated that a thicker diffusion layer may lead to a further increase in coating adhesion, which can be conducted by extended the remelting time. However, some unexpected outcomes, such as oxidation and/or grain coarsening, may occur to the remelted NiCrBSi coating.

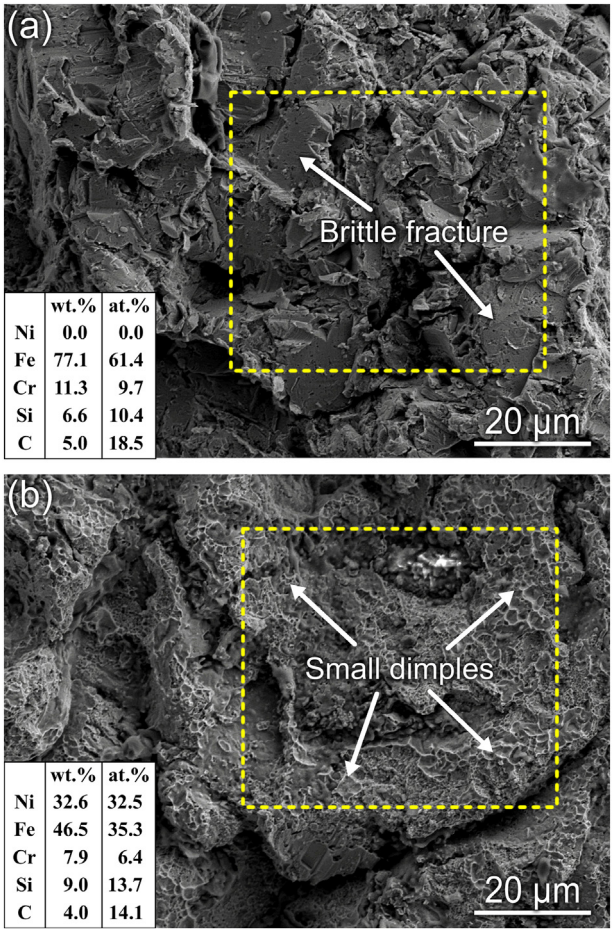

	wt.%	at.%
Ni	0.0	0.0
Fe	77.1	61.4
Cr	11.3	9.7
Si	6.6	10.4
C	5.0	18.5

	wt.%	at.%
Ni	32.6	32.5
Fe	46.5	35.3
Cr	7.9	6.4
Si	9.0	13.7
C	4.0	14.1

Fig. 10. SEM images for the fracture morphologies of (a) the as-sprayed and (b) remelted NiCrBSi coatings.

3.5. Wear performance

Fig. 11 shows the wear test results of the 2Cr13 substrate, the as-sprayed and remelted NiCrBSi coatings at 5 mm/s or 10 mm/s sliding speed. The 2Cr13 substrate exhibits the highest friction coefficients (0.70 at 5 mm/s sliding speed and 0.76 at 10 mm/s sliding speed, respectively) among the three tested samples (Fig. 11a). The friction coefficients of the as-sprayed NiCrBSi coating, 0.55 at 5 mm/s sliding speed and 0.58 at 10 mm/s sliding speed, are much lower than those of the substrate (Fig. 11a), indicating that the as-sprayed NiCrBSi coating has better wear resistance than the 2Cr13 substrate. Furthermore, the remelted NiCrBSi coating possesses the substantially lower friction coefficients (0.42 at 5 mm/s sliding speed and 0.52 at 10 mm/s sliding speed, respectively) than those of the as-sprayed counterpart (Fig. 11a). Similar results are found in the wear volumes of the tested samples. At the 5 mm/s sliding speed, the wear volumes of the 2Cr13 substrate, the as-sprayed and remelted NiCrBSi coatings are 0.156 mm^3, 0.76 mm^3, and 0.50 mm^3, respectively (Fig. 11b). As the sliding speed increases, the wear volumes of the 2Cr13 substrate, the as-sprayed and remelted NiCrBSi coatings also increase to 0.172 mm^3, 0.085 mm^3, and 0.059 mm^3, respectively (Fig. 11b). Therefore, it can be concluded that the remelted NiCrBSi coating has much better wear resistance than the as-sprayed NiCrBSi coating. Similar to the results of friction coefficients, higher sliding speed leads to greater wear volumes for all tested sample. Meanwhile, the wear resistance of the 2Cr13 substrate, the as-sprayed and remelted NiCrBSi coatings coincides with the variation in their hardness (Fig. 8).

Fig. 12 represents the worn surfaces of the substrate, the as-sprayed and remelted NiCrBSi coatings after the wear tests. The substrate shows

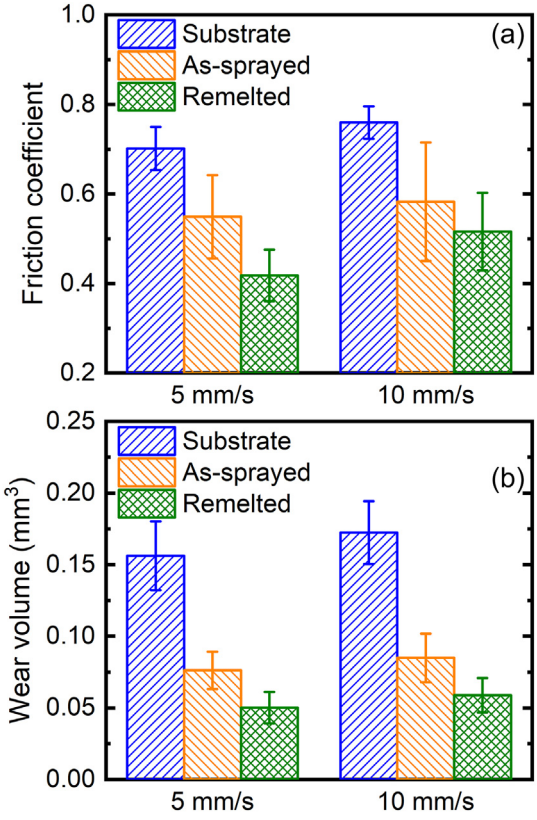

Fig. 11. Wear performance of the substrate, the as-sprayed and remelted NiCrBSi coatings: (a) friction coefficient and (b) wear volume.

a considerable number of severe ploughs and a few of micro-cracks at 5 mm/s sliding speed (Fig. 12a). The ploughs are caused by the abrasive particles provided by the wear debris [69]. Hence, it indicates that the 2Cr13 substrate undergoes abrasive wear. As seen in Fig. 12b, wear becomes more severe on the substrate at the sliding speed of 10 mm/s and delamination can be clearly observed on the worn surface of the substrate. The surface of the substrate becomes rugged. As a result, fretting wear takes place [70,71]. Meanwhile, it could also be found that the plough becomes deeper compared with the counterpart tested under the sliding speed of 5 mm/s. Therefore, scoring wear also takes place besides abrasive wear. Such a result is in line with the friction coefficients and wear volumes of the substrate presented in Fig. 11, specifying the substrate has a poor wear resistance. The worn surface of the as-sprayed NiCrBSi coating is much flatter than that of the substrate, indicating that the as-sprayed NiCrBSi coating has a better wear resistance (Fig. 11a and c). However, the as-sprayed NiCrBSi coating shows lots of micro-cracks on the worn surface (Fig. 12c). Some unmelted particles surrounded by voids are indicated by white arrows in Fig. 12c. As mentioned above, the stacking of the unmelted particles can generate pores in the as-sprayed NiCrBSi coating. Therefore, such a morphology containing lots of voids and pores is prone to cause stress concentration by shear deformation, leading to the formation of micro-cracks in the as-sprayed NiCrBSi coating during wear test [7]. Furthermore, the abrasive wear is very mild on the worn surface of the as-sprayed NiCrBSi as indicated by the solid arrow in Fig. 12c. When the sliding speed increases to 10 mm/s, severe abrasive wear is observed on the worn surface of the as-sprayed NiCrBSi coating besides unmelted particle and micro-cracks (Fig. 12d). This finding illustrates that more debris is produced during the wear test at the 10 mm/s sliding speed. At higher sliding speed, stress is more prone to concentrate at the locations of pores and voids in the as-sprayed NiCrBSi coating, thereby leading to a more severe abrasive wear. In the comparison of the worn surfaces, the remelted NiCrBSi coating shows a much intact worn surface with

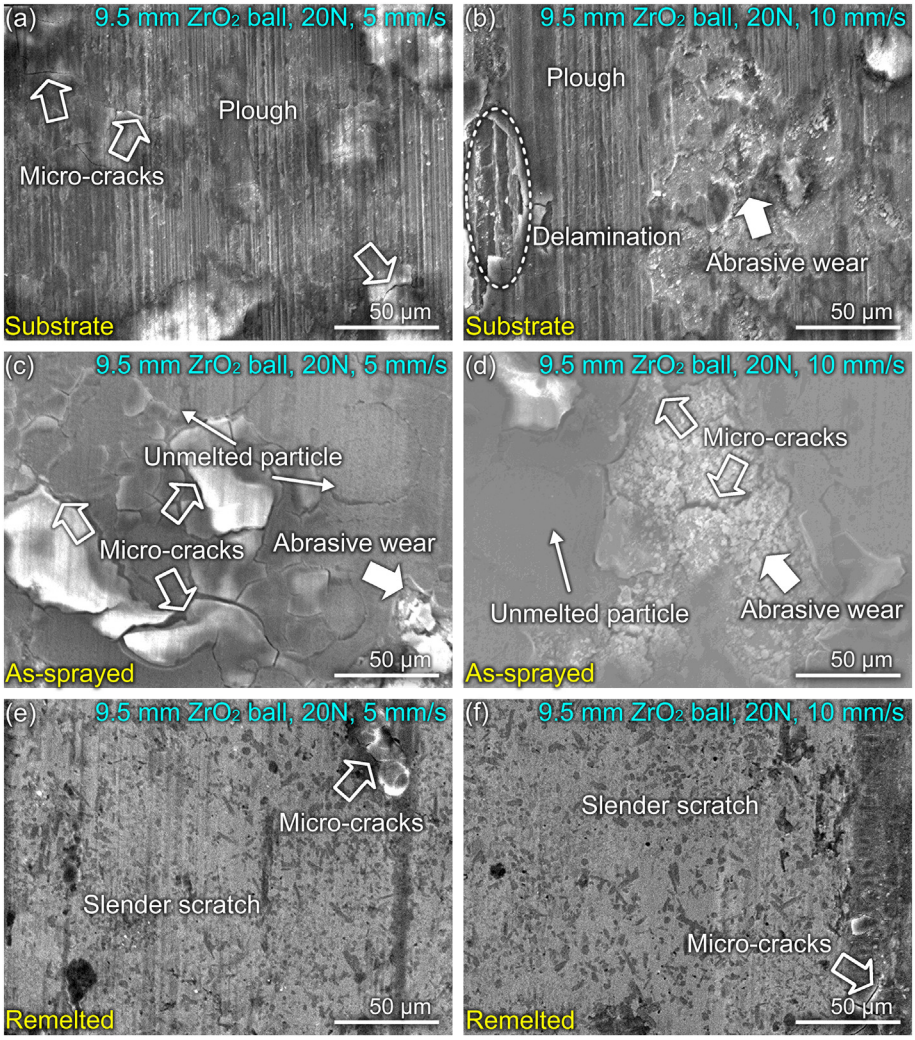

Fig. 12. SEM images for worn surfaces of (a), (b) the substrate as-sprayed sample, (c), (d) the as-sprayed and (e), (f) remelted NiCrBSi coatings at 5 mm/s and 10 mm/s sliding speeds.

the slender scratch. Micro-cracks in the remelted NiCrBSi coating are significantly less than those in the as-sprayed NiCrBSi coating (Fig. 12e and f). No abrasive wear is observed on the worn surface of the remelted NiCrBSi coating. It is reasonable that the remelted NiCrBSi coating has the highest hardness among the tested samples. The increase in hardness reduces the contact area between the friction counterpart and the tested sample surface, thereby resulting in the less shear deformation of the tested sample. Meanwhile, the remelted NiCrBSi coating has significantly lower porosity than the as-sprayed counterpart. Therefore, stress concentration is also lower in the remelted NiCrBSi coating. For these reasons, the remelted NiCrBSi coating possesses better wear resistance than the as-sprayed counterpart.

3.6. Comparison among other remelting methods

As there are almost no reports on the bonding strength of the remelted NiCrBSi coatings by the bonding strength test, it is hard to compare the bonding strength of the NiCrBSi coatings adhere to different substrates. In order to give a universal comparison between the NiCrBSi coatings remelted by various methods, hardness increment percentage is selected to stress on the strengthening effect of the remelting process since the absolute hardness value may be varied according to their specific chemical compositions. Fig. 13 summarizes the hardness increment percentage of the remelted NiCrBSi coatings extracted from the literature [10,11,18–20,22–25] as well as from this work. Due to the different spraying and remelting methods adopted, the results are varied from 2.8% to 60.3% in Fig. 13. The outcome of this work (22.2%) is in the middle of the hardness increment percentage range reported. However, the remelting experiments are repeated and the outcomes are highly concentrated using the same spraying and remelting processing parameters, indicating the reliability and the reproducibility of this method. In comparison, the quality of the remelted NiCrBSi coatings processed by laser remelting also depends on the processing parameters. Apparently, the lowest hardness increment percentage (2.8%) of the remelted NiCrBSi coating is processed by laser remelting [25], indicating that inapposite laser processing parameters may not enhance the performance of the remelted NiCrBSi coating. By contrast, it was reported that the hardness increment percentages also increase to 41% and 54%, respectively [18,20]. In the meantime, the wear resistance decrement in the NiCrBSi coatings remelted by various methods is summarized in Table 3. As different wear tests are conducted in the literature [19,20,23–25], wear volume, wear loss or wear rate are selected to investigate the decrements in the wear resistance of the remelted NiCrBSi coatings. Although these results cannot give a quantitative comparison in the decrements in wear resistance of the remelted NiCrBSi coatings prepared by various methods, one can still find that all remelting methods have significant strengthening effects on the wear resistance of the NiCrBSi coatings. The remelted NiCrBSi coating has 30.7% decrement compared to the as-sprayed NiCrBSi

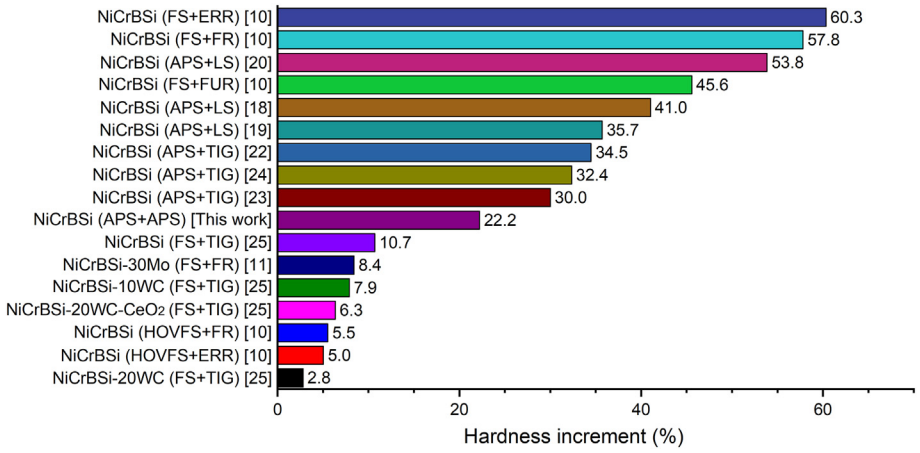

Fig. 13. Comparison of hardness increment percentages of the remelted NiCrBSi coatings extracted from literature [10,11,18–20,22–25] and this work. HVOFS: high velocity oxygen fuel spraying; FS: flame spraying; APS: atmospheric plasma spraying; FR: flame remelting; LS: laser remelting; FUR: furnace remelting; ERR: electric resistance remelting; TIG: tungsten inert gas remelting; PR: plasma gun remelting. The amounts of the additions are in wt%.

coating in this work. The decrement in wear resistance of the remelted NiCrBSi coating in this work is not very high among the investigated values as listed in Table 3. However, using the same equipment to spray and remelt the coatings (even other materials) is rather convenient in factual applications.

Based on the results obtained in this work, one can conclude that the changes in the properties of the as-sprayed and remelted NiCrBSi coatings can be attributed to the variations in the microstructure or morphology. First, the elimination of the pores and lamellar boundaries can significantly enhance the cohesion of the NiCrBSi coatings, thereby increasing the hardness and wear resistance properties (Figs. 4, 8 and 11). Second, the formation of the metallurgical bonding resulted from the interdiffusion between the coating and the substrate extremely enhances the coating adhesion (Figs. 5 and 9). Third, the microstructure may coarse under the conditions of excessive heat input and the relatively slow cooling rate after remelting (Figs. 6 and 7). As demonstrated in Ref. [7], the hardness of the NiCrBSi coating would decrease during grain growth. In comparison, the laser has a higher energy density compared with the plasma gun, resulting in a faster heating/cooling rate and a refined microstructure during remelting [18,72,73]. As a result, higher hardness and higher hardness increment are obtained by laser remelting [18,20]. Unfortunately, not all the laboratory or factory owns laser equipment. The plasma remelted NiCrBSi coating used in this work is successfully prepared after several attempts. As such, selecting a set of appropriate remelting parameters to control the heat input is also a critical consideration by using this method. Above all, considering the reliability and the convenience of this method and the enhanced mechanical properties of the remelted NiCrBSi coating, one can expect that a wider range of materials (such as refractory metals and ceramics) may be selected as remelted coating materials since plasma spray possesses a significantly higher energy output.

4. Conclusions

In this work, the plasma sprayed NiCrBSi coating was remelted by using the plasma gun in an automatic mode. Microstructures and mechanical properties (such as hardness, bonding strength and wear performance) of the as-sprayed and remelted NiCrBSi are systematically characterized. Furthermore, a comparison among the different remelting methods was conducted. Some key conclusions are drawn as follows:

(1) Microstructural observations indicate that the as-sprayed NiCrBSi coating contains a meta-stable phase (Cr_3B_4) and the amorphous phase, which results in the fast cooling rate of the particles during deposition. After remelting, because of a relatively low cooling rate, the remelted NiCrBSi only possesses crystal phases of γ-Ni, Cr_7C_3, Cr_3C_2, Ni_3B and CrB.
(2) Porosity is significantly reduced from 2.7% in the as-sprayed NiCrBSi coating to 0.8% in the remelted one after remelting. Moreover, the remelting process causes the transformation of the coating/substrate interface from mechanical interlocking to metallurgical bonding. Due to high temperature during the remelting process (over 1500 °C), the remelted NiCrBSi coating has larger grains than the as-sprayed counterpart.
(3) The mechanical properties of the remelted NiCrBSi coating are significantly enhanced by the remelting process. The hardness and bonding strength of the remelted NiCrBSi coating are 803 $HV_{0.5}$ and 165 MPa, respectively, which are about 22% and 516% higher than those of the as-sprayed NiCrBSi counterpart (hardness: 657 $HV_{0.5}$; bonding strength: 32 MPa). Also, the remelted NiCrBSi coating possesses a lower friction coefficient and wear volume than the as-sprayed NiCrBSi counterpart at both 5 mm/s and 10 mm/s slide speed.
(4) A comparison for the hardness and hardness increment percentages

Table 3
A comparison of wear performance of NiCrBSi-based coating by various spraying and remelting methods. FS: flame spraying; APS: atmospheric plasma spraying; FR: flame remelting; LS: laser remelting; TIG: tungsten inert gas remelting; PR: plasma gun remelting. The amounts of the additions are in wt%.

Materials	Methods	Comparison	Wear conditions	Increments	Ref.
NiCrBSi	APS + TIG	Wear volume	4 mm GCr15 ball, 30 N, 40 mm/s, 48,000 mm	83.0%	[24]
NiCrBSi	APS + LS	Wear volume	5 mm Si3N4 ball, 50 N, 94 mm/s, 84,780 mm	64.2%	[19]
NiCrBSi	APS + TIG	Wear loss	40 mm GCr15 ball, 300 N, 83.7 mm/s, 1,506,600 mm	63.8%	[23]
NiCrBSi	APS + LS	Wear rate	6 mm 100Cr6 ball, 2 N, 500 mm/s, 10,000,000 mm	54.1%	[20]
NiCrBSi	FS + TIG	Wear rate	600 grits paper, 20 N, 142 mm/s, 21,300 mm	18.8%	[25]
NiCrBSi-10WC	FS + TIG	Wear rate	600 grits paper, 20 N, 142 mm/s, 21,300 mm	21.6%	[25]
NiCrBSi-20WC	FS + TIG	Wear rate	600 grits paper, 20 N, 142 mm/s, 21,300 mm	28.9%	[25]
NiCrBSi-20WC-0.8CeO_2	FS + TIG	Wear rate	600 grits paper, 20 N, 142 mm/s, 21,300 mm	14.5%	[25]
NiCrBSi-30%Mo	APS + FR	Wear volume	4 mm AISI ball, 40 N, 40 mm/s, 48,000 mm	80.2%	[11]
NiCrBSi	APS + PR	Wear volume	9.5 mm ZrO_2 ball, 20 N, 10 mm/s, 12,000 mm	30.7%	This work

of the remelted NiCrBSi coatings extracted from literature and this work is conducted. Although the hardness and hardness increment percentages of the remelted NiCrBSi coating in this work are not the highest among the extracted data, the remelting method by plasma gun in an automatic mode is reliable, reproducible and convenient with no need for additional equipment. Therefore, the remelting process used in this work is prominently useful for wider industrial applications.

Acknowledgment

The authors would like to acknowledge a financial support provided by National Natural Science Foundation of China (51601075 and 51375218), China Postdoctoral Science Foundation Funded Project (2017M611751), Open Foundation of Guangxi Key Laboratory of Processing for Non-ferrous Metals and Featured Materials, Guangxi University (Grant No. GXYSOF1801), and Jiangsu University of Science and Technology Overseas Research & Training Program for University Prominent Young & Middle-aged Teachers.

References

[1] C. Shi, J. Lei, S. Zhou, X. Dai, L.C. Zhang, Microstructure and mechanical properties of carbon fibers strengthened Ni-based coatings by laser cladding: the effect of carbon fiber contents, J. Alloys Compd. 744 (2018) 146–155.
[2] J. Lei, C. Shi, S. Zhou, Z. Gu, L.C. Zhang, Enhanced corrosion and wear resistance properties of carbon fiber reinforced Ni-based composite coating by laser cladding, Surf. Coat. Technol. 334 (2018) 274–285.
[3] J. Li, L. Pan, Q. Fu, Y. Zhou, N. Guo, Wettability and corrosion behavior of a Ni coating on 304 stainless steel surface, Surf. Coat. Technol. 357 (2019) 740–747.
[4] M. Mirak, A. Akbari, Microstructural characterization of electrodeposited and heat-treated Ni-B coatings, Surf. Coat. Technol. 349 (2018) 442–451.
[5] A. Salimi, S. Sanjabi, Infiltration brazed core-shell WC@NiP/NiCrBSi composite cladding, Surf. Coat. Technol. 352 (2018) 59–73.
[6] Y. Zhou, J. Zhang, Z. Xing, H. Wang, Z. Lv, Microstructure and properties of NiCrBSi coating by plasma cladding on gray cast iron, Surf. Coat. Technol. 361 (2019) 270–279.
[7] L.-Y. Chen, T. Xu, S. Lu, Z.-X. Wang, S. Chen, L.-C. Zhang, Improved hardness and wear resistance of plasma sprayed nanostructured NiCrBSi coating via short-time heat treatment, Surf. Coat. Technol. 350 (2018) 436–444.
[8] L.-Y. Chen, T. Xu, H. Wang, P. Sang, S. Lu, Z.-X. Wang, S. Chen, L.-C. Zhang, Phase interaction induced texture in a plasma sprayed-remelted NiCrBSi coating during solidification: an electron backscatter diffraction study, Surf. Coat. Technol. 358 (2019) 467–480.
[9] L.H. Tian, W. Xiong, C. Liu, S. Lu, M. Fu, Microstructure and wear behavior of atmospheric plasma-sprayed AlCoCrFeNiTi high-entropy alloy coating, J. Mater. Eng. Perform. 25 (2016) 5513–5521.
[10] Š. Houdková, E. Smazalová, M. Vostřák, J. Schubert, Properties of NiCrBSi coating, as sprayed and remelted by different technologies, Surf. Coat. Technol. 253 (2014) 14–26.
[11] X.C. Yang, G.L. Li, H.D. Wang, T.S. Dong, J.J. Kang, Effect of flame remelting on microstructure and wear behaviour of plasma sprayed NiCrBSi-30%Mo coating, Surf. Eng. 34 (2018) 181–188.
[12] H. Vasudev, L. Thakur, A. Bansal, H. Singh, S. Zafar, High temperature oxidation and erosion behaviour of HVOF sprayed bi-layer Alloy-718/NiCrAlY coating, Surf. Coat. Technol. 362 (2019) 366–380.
[13] A.G. Mora-García, H. Ruiz-Luna, M. Mosbacher, R. Popp, U. Schulz, U. Glatzel, J. Muñoz-Saldaña, Microstructural analysis of Ta-containing NiCoCrAlY bond coats deposited by HVOF on different Ni-based superalloys, Surf. Coat. Technol. 354 (2018) 214–225.
[14] H. Singh, B.S. Sidhu, D. Puri, S. Prakash, Use of plasma spray technology for deposition of high temperature oxidation/corrosion resistant coatings - a review, Mater. Corros. 58 (2007) 92–102.
[15] A. Vardelle, C. Moreau, J. Akedo, H. Ashrafizadeh, C.C. Berndt, J.O. Berghaus, M. Boulos, J. Brogan, A.C. Bourtsalas, A. Dolatabadi, The 2016 thermal spray roadmap, J. Therm. Spray Technol. 25 (2016) 1376–1440.
[16] Z. Bergant, U. Trdan, J. Grum, Effect of high-temperature furnace treatment on the microstructure and corrosion behavior of NiCrBSi flame-sprayed coatings, Corros. Sci. 88 (2014) 372–386.
[17] R. Gonzalez, M.A. Garcia, I. Penuelas, M. Cadenas, M. del R. Fernandez, A.H. Battez, D. Felgueroso, Microstructural study of NiCrBSi coatings obtained by different processes, Wear 263 (2007) 619–624.
[18] N. Serres, F. Hlawka, S. Costil, C. Langlade, F. Machi, A. Cornet, Combined plasma spray and in situ laser melting treatment of NiCrBSi powder, J. Optoelectron. Adv. Mater. 12 (2010) 505–510.
[19] H. Guo, Z. Tian, Y. Huang, H. Yang, Microstructure and tribological properties of laser-remelted Ni-based WC coatings obtained by plasma spraying, J. Russ. Laser Res. 36 (2015) 48–58.
[20] N. Serres, F. Hlawka, S. Costil, C. Langlade, F. Machi, An investigation of the mechanical properties and wear resistance of NiCrBSi coatings carried out by in situ laser remelting, Wear 270 (2011) 640–649.
[21] Z. Bergant, J. Grum, Quality improvement of flame sprayed, heat treated, and remelted NiCrBSi coatings, J. Therm. Spray Technol. 18 (2009) 380–391.
[22] L. Guo-lu, L. Ya-long, D. Tian-shun, F. Bin-Guo, W. Hai-dou, Z. Xiao-dong, Z. Xiu-kai, Microstructure and interface characteristics of NiCrBSi thick coating remelted by TIG process, Vacuum 156 (2018) 440–448.
[23] L. Ya-long, D. Tian-shun, L. Guo-lu, W. Hai-dou, F. Bin-Guo, Z. Xiao-dong, Microstructure evolution and properties of NiCrBSi thick coating remelted by gas tungsten arc, Surf. Coat. Technol. 349 (2018) 260–271.
[24] G. Li, Y. Li, T. Dong, H. Wang, X. Zheng, X. Zhou, Microstructure and wear resistance of TIG remelted NiCrBSi thick coatings, Adv. Mater. Sci. Eng. 2018 (2018) 8979678.
[25] B.M. Dhakar, D.K. Dwivedi, S.P. Sharma, Studies on remelting of tungsten carbide and rare earth modified nickel base alloy composite coating, Surf. Eng. 28 (2012) 73–80.
[26] M.R. Karimi, H.R. Salimijazi, M.A. Golozar, Effects of remelting processes on porosity of NiCrBSi flame sprayed coatings, Surf. Eng. 32 (2016) 238–243.
[27] J. Chen, Y. Dong, L. Wan, Y. Yang, Z. Chu, J. Zhang, J. He, D. Li, Effect of induction remelting on the microstructure and properties of in situ TiN-reinforced NiCrBSi composite coatings, Surf. Coat. Technol. 340 (2018) 159–166.
[28] R.R. González, M. Cadenas, R.R. Fernández, J.L. Cortizo, E. Rodríguez, Wear behaviour of flame sprayed NiCrBSi coating remelted by flame or by laser, Wear 262 (2007) 301–307.
[29] L. Chai, K. Chen, Y. Zhi, K.L. Murty, L.Y. Chen, Z. Yang, Nanotwins induced by pulsed laser and their hardening effect in a Zr alloy, J. Alloys Compd. 748 (2018) 163–170.
[30] L.-C. Zhang, Y. Liu, S. Li, Y. Hao, Additive manufacturing of titanium alloys by electron beam melting: a review, Adv. Eng. Mater. 20 (2018) 1700842.
[31] J.J. Tian, S.W. Yao, X.T. Luo, C.X. Li, C.J. Li, An effective approach for creating metallurgical self-bonding in plasma-spraying of NiCr-Mo coating by designing shell-core-structured powders, Acta Mater. 110 (2016) 19–30.
[32] D.T. Hawkins, The B-Cr (boron-chromium) system, Bull. Alloy Phase Diagrams 2 (1981) 108–109.
[33] L.C. Zhang, K.B. Kim, P. Yu, W.Y. Zhang, U. Kunz, J. Eckert, Amorphization in mechanically alloyed (Ti, Zr, Nb)-(Cu, Ni)-Al equiatomic alloys, J. Alloys Compd. 428 (2007) 157–163.
[34] L.C. Zhang, J. Xu, Glass-forming ability of melt-spun multicomponent (Ti, Zr, Hf)–(Cu, Ni, Co)–Al alloys with equiatomic substitution, J. Non-Cryst. Solids 347 (2004) 166–172.
[35] L.C. Zhang, Z.Q. Shen, J. Xu, Mechanically milling-induced amorphization in Sn-containing Ti-based multicomponent alloy systems, Mater. Sci. Eng. A 394 (2005) 204–209.
[36] L.C. Zhang, J. Xu, E. Ma, Mechanically alloyed amorphous $Ti_{50}(Cu_{0.45}Ni_{0.55})_{44}$–$xAl_xSi_4B_2$ alloys with supercooled liquid region, J. Mater. Res. 17 (2002) 1743–1749.
[37] M. Calin, L.C. Zhang, J. Eckert, Tailoring of microstructure and mechanical properties of a Ti-based bulk metallic glass-forming alloy, Scr. Mater. 57 (2007) 1101–1104.
[38] P. Yu, L.C. Zhang, W.Y. Zhang, J. Das, K.B. Kim, J. Eckert, Interfacial reaction during the fabrication of $Ni_{60}Nb_{40}$ metallic glass particles-reinforced Al based MMCs, Mater. Sci. Eng. A 444 (2007) 206–213.
[39] L.C. Zhang, J. Xu, E. Ma, Consolidation and properties of ball-milled $Ti_{50}Cu_{18}Ni_{22}Al_4Sn_6$ glassy alloy by equal channel angular extrusion, Mater. Sci. Eng. A 434 (2006) 280–288.
[40] L.-C. Zhang, J. Xu, J. Eckert, Thermal stability and crystallization kinetics of mechanically alloyed TiC/Ti-based metallic glass matrix composite, J. Appl. Phys. 100 (2006) 033514.
[41] L.C. Zhang, Z.Q. Shen, J. Xu, Glass formation in a (Ti,Zr,Hf)-(Cu,Ni,Ag)-Al high-order alloy system by mechanical alloying, J. Mater. Res. 18 (2003) 2141–2149.
[42] X.C. Zhang, B.S. Xu, S.T. Tu, F.Z. Xuan, H.D. Wang, Y.X. Wu, Effect of spraying power on the microstructure and mechanical properties of supersonic plasma-sprayed Ni-based alloy coatings, Appl. Surf. Sci. 254 (2008) 6318–6326.
[43] L. Liu, H. Xu, J. Xiao, X. Wei, G. Zhang, C. Zhang, Effect of heat treatment on structure and property evolutions of atmospheric plasma sprayed NiCrBSi coatings, Surf. Coat. Technol. 325 (2017) 548–554.
[44] L.-C. Zhang, L.-Y. Chen, A review on biomedical titanium alloys: recent progress and prospect, Adv. Eng. Mater. 21 (2019) 1801215.
[45] A. Bahramian, M. Eyraud, F. Vacandio, P. Knauth, Improving the corrosion properties of amorphous Ni-P thin films using different additives, Surf. Coat. Technol. 345 (2018) 40–52.
[46] I. Hemmati, J.C. Rao, V. Ocelik, J.T.M. De Hosson, Electron microscopy characterization of Ni-Cr-B-Si-C laser deposited coatings, Microsc. Microanal. 19 (2013) 120–131.
[47] A. Vencl, S. Arostegui, G. Favaro, F. Zivic, M. Mrdak, S. Mitrović, V. Popovic, Evaluation of adhesion/cohesion bond strength of the thick plasma spray coatings by scratch testing on coatings cross-sections, Tribol. Int. 44 (2011) 1281–1288.
[48] Y.Y. Wang, C.J. Li, A. Ohmori, Influence of substrate roughness on the bonding mechanisms of high velocity oxy-fuel sprayed coatings, Thin Solid Films 485 (2005) 141–147.
[49] Y.Y. Wang, C.J. Li, A. Ohmori, Examination of factors influencing the bond strength of high velocity oxy-fuel sprayed coatings, Surf. Coat. Technol. 200 (2006) 2923–2928.
[50] C.-J. Li, Y.-Y. Wang, Effect of particle state on the adhesive strength of HVOF sprayed metallic coating, J. Therm. Spray Technol. 11 (2002) 523–529.
[51] N. Serres, F. Hlawka, S. Costil, C. Langlade, F. MacHi, Microstructures and

mechanical properties of metallic NiCrBSi and composite NiCrBSi-WC layers manufactured via hybrid plasma/laser process, Appl. Surf. Sci. 257 (2011) 5132–5137.
[52] M.R. Fernández, A. García, J.M. Cuetos, R. González, A. Noriega, M. Cadenas, Effect of actual WC content on the reciprocating wear of a laser cladding NiCrBSi alloy reinforced with WC, Wear 324–325 (2015) 80–89.
[53] Y. Chen, J. Zhang, N. Dai, P. Qin, H. Attar, L.-C. Zhang, Corrosion behaviour of selective laser melted Ti-TiB biocomposite in simulated body fluid, Electrochim. Acta 232 (2017) 89–97.
[54] C.D. Rabadia, Y.J. Liu, L. Wang, H. Sun, L.C. Zhang, Laves phase precipitation in Ti-Zr-Fe-Cr alloys with high strength and large plasticity, Mater. Des. 154 (2018) 228–238.
[55] X. Lu, Y.F. Zhou, X.L. Xing, B. Wang, Q.X. Yang, S.Y. Gao, Surface additive manufacturing of Ni-based superalloy/H13 steel system by laser depositing: microstructure, microhardness and flexural response, Surf. Coat. Technol. 337 (2018) 525–535.
[56] J.C. Pereira, J.C. Zambrano, E. Rayón, A. Yañez, V. Amigó, Mechanical and microstructural characterization of MCrAlY coatings produced by laser cladding: the influence of the Ni, Co and Al content, Surf. Coat. Technol. 338 (2018) 22–31.
[57] L.Y. Chen, P. Shen, L. Zhang, S. Lu, L. Chai, Z. Yang, L.C. Zhang, Corrosion behavior of non-equilibrium Zr-Sn-Nb-Fe-Cu-O alloys in high-temperature 0.01 M LiOH aqueous solution and degradation of the surface oxide films, Corros. Sci. 136 (2018) 221–230.
[58] L. Chen, J. Li, Y. Zhang, W. Lu, L.C. Zhang, L. Wang, D. Zhang, Effect of low-temperature pre-deformation on precipitation behavior and microstructure of a Zr-Sn-Nb-Fe-Cu-O alloy during fabrication, J. Nucl. Sci. Technol. 53 (2016) 496–507.
[59] D.P. Song, J. Yang, Y.X. Wang, X.B. Zhu, Magnetic and ferroelectric properties of Aurivillius phase Bi7Fe3Ti3O21 and their doped films, Ceram. Int. 43 (2017) 17148–17152.
[60] D. Song, J. Yang, B. Yang, L. Chen, F. Wang, X. Zhu, Evolution of structure and ferroelectricity in Aurivillius Bi4Bin − 3Fen − 3Ti3O 3n + 3 thin films, J. Mater. Chem. C 6 (2018) 8618–8627.
[61] H.-Y. Yang, Z. Wang, S.-L. Shu, J.-B. Lu, Effect of Ta addition on the microstructures and mechanical properties of in situ bi-phase (TiB_2-TiCxNy)/(Ni-Ta) cermets, Ceram. Int. 45 (2019) 4408–4417.
[62] T. Tokunaga, K. Nishio, H. Ohtani, M. Hasebe, Thermodynamic assessment of the Ni-Si system by incorporating ab initio energetic calculations into the CALPHAD approach, Calphad Comput. Coupling Phase Diagrams Thermochem. 27 (2003) 161–168.
[63] T. Ezaz, H. Sehitoglu, Coupled shear and shuffle modes during twin growth in B2-NiTi, Appl. Phys. Lett. 98 (2011) 241906.
[64] L. Wang, L. Xie, L.-C. Zhang, L. Chen, Z. Ding, Y. Lv, W. Zhang, W. Lu, D. Zhang, Microstructure evolution and superelasticity of layer-like NiTiNb porous metal prepared by eutectic reaction, Acta Mater. 143 (2018) 214–226.
[65] Y.J. Liu, S.J. Li, L.C. Zhang, Y.L. Hao, T.B. Sercombe, Early plastic deformation behaviour and energy absorption in porous β-type biomedical titanium produced by selective laser melting, Scr. Mater. 153 (2018) 99–103.
[66] H. Attar, M. Bönisch, M. Calin, L.C. Zhang, K. Zhuravleva, A. Funk, S. Scudino, C. Yang, J. Eckert, Comparative study of microstructures and mechanical properties of in situ Ti–TiB composites produced by selective laser melting, powder metallurgy, and casting technologies, J. Mater. Res. 29 (2014) 1941–1950.
[67] Y. Liu, S. Li, W. Hou, S. Wang, Y. Hao, R. Yang, T.B. Sercombe, L.C. Zhang, Electron beam melted beta-type Ti-24Nb-4Zr-8Sn porous structures with high strength-to-modulus ratio, J. Mater. Sci. Technol. 32 (2016) 505–508.
[68] S. Zhao, S.J. Li, S.G. Wang, W.T. Hou, Y. Li, L.C. Zhang, Y.L. Hao, R. Yang, R.D.K.K. Misra, L.E. Murr, Compressive and fatigue behavior of functionally graded Ti-6Al-4V meshes fabricated by electron beam melting, Acta Mater. 150 (2018) 1–15.
[69] X. Qin, X. Guo, J. Lu, L. Chen, J. Qin, W. Lu, Erosion-wear and intergranular corrosion resistance properties of AISI 304L austenitic stainless steel after low-temperature plasma nitriding, J. Alloys Compd. 698 (2017) 1094–1101.
[70] Y.S. Zhang, W.L. Li, G. Wang, L.C. Zhang, B. Yao, Z. Han, Formation of thick nanocrystalline surface layer on copper during oscillating sliding, Mater. Lett. 68 (2012) 432–434.
[71] Y.S. Zhang, H.Z. Niu, L.C. Zhang, X.F. Bai, X.M. Zhang, P.X. Zhang, Grain coarsening behavior in a nanocrystalline copper subjected to sliding friction, Mater. Lett. 123 (2014) 261–264.
[72] L.J. Chai, S.Y. Wang, H. Wu, N. Guo, H.C. Pan, L.Y. Chen, K.L. Murty, B. Song, α → β transformation characteristics revealed by pulsed laser-induced non-equilibrium microstructures in duplex-phase Zr alloy, Sci. China Technol. Sci. 60 (2017) 1255–1262.
[73] Y.J. Liu, Z. Liu, Y. Jiang, G.W. Wang, Y. Yang, L.C. Zhang, Gradient in microstructure and mechanical property of selective laser melted AlSi10Mg, J. Alloys Compd. 735 (2018) 1414–1421.